PAPER

Comparative study of deuterium retention in irradiated Eurofer and Fe–Cr from a new ion implantation materials facility

IOP Publishing | International Atomic Energy Agency Nuclear Fusion

Nucl. Fusion **60** (2020) 016024 (10pp) https://doi.org/10.1088/1741-4326/ab546e

Comparative study of deuterium retention in irradiated Eurofer and Fe–Cr from a new ion implantation materials facility

A. Hollingsworth[1,a], M.Yu. Lavrentiev[1], R. Watkins[1], A.C. Davies[1], S. Davies[1], R. Smith[1], D.R. Mason[1], A. Baron-Wiechec[1,2,3], Z. Kollo[1], J. Hess[1], I. Jepu[4], J. Likonen[5], K. Heinola[6], K. Mizohata[6], E. Meslin[7], M.-F. Barthe[8], A. Widdowson[1], I.S. Grech[1], K. Abraham[1], E. Pender[1], A. McShee[1], Y. Martynova[9], M. Freisinger[9] and A. De Backer[1]

[1] UKAEA-CCFE, Culham Science Centre, Abingdon, OX14 3DB, United Kingdom of Great Britain and Northern Ireland
[2] Technion, Israel Institute of Technology, Haifa 32000, Israel
[3] Guangdong Technion, Israel Institute of Technology, Shantou 515063, China
[4] Laboratory of Low Temperature Plasma, National Institute for Laser, Plasma and Radiation Physics, Magurele, Romania
[5] VTT Technical Research Centre of Finland, Espoo, Finland
[6] Department of Physics, University of Helsinki, Helsinki, Finland
[7] DEN-Service de Recherches de Métallurgie Physique, CEA, Université Paris-Saclay, F-91191 Gif-sur-Yvette, France
[8] CEMHTI/CNRS, Université d'Orléans, Orléans, France
[9] Forschungszentrum Jülich GmbH, 52425 Jülich, Germany

E-mail: Anthony.Hollingsworth@ukaea.uk

Received 27 June 2019, revised 7 October 2019
Accepted for publication 5 November 2019
Published 25 November 2019

Abstract

A new facility to study the interaction of hydrogen isotopes with nuclear fusion-relevant first wall materials, and their retention and release, has been produced. The new facility allows for implanting a range of gases into samples, including tritium. An accurate study of isotope effects, such as the isotopic exchange in damaged microstructure, has previously been difficult due to a background signal of light hydrogen. This new capability will allow virtually background free measurements using tritium and deuterium. The design and build of this facility are described and commissioning results are presented. Within the UKAEA-led tritium retention in controlled and evolving microstructure (TRiCEM) project, this facility is used for the comparative study of deuterium retention in self-ion irradiated Eurofer steel and Fe–Cr alloy. Self-ion bombardment with energies of 0.5 MeV is used to mimic the defects created by neutrons in fusion power plants and the created traps are then filled with deuterium in the new facility. Implanted samples are analysed using thermal desorption spectrometry (TDS), secondary ion mass spectrometry (SIMS), and transmission electron microscopy. Results on the total deuterium content as a function of time, TDS spectra and SIMS analysis are presented. A comparison of the results for Eurofer and Fe–Cr revealed several differences. While some of them may be due to experimental details like different time delays between exposure and analysis, others, such as deuterium retention as function of dose, might be genuine and require further studies.

Keywords:deuterium, tritium, Eurofer, iron-chromium, implanting, retention

(Some figures may appear in colour only in the online journal)

[a] Author to whom any correspondence should be addressed.

1. Introduction

In present nuclear fusion devices and in the future fusion power plants, the plasma interacts with the first wall, and affects the blanket and the divertor. In the next-step fusion device ITER, the main materials facing the plasma are beryllium and tungsten [1–3], whereas in the future demonstration fusion reactor DEMO the first wall material mix comprises of tungsten and reduced-activation ferritic-martensitic (RAFM) steels [4–6]. The structural materials of the vacuum vessel are austenitic steels but research on advanced materials like the RAFM steel Eurofer97 is ongoing. The engineering and research challenges are the control and understanding of the evolution of the mechanical properties and the tritium retention of these materials which face the extreme conditions of the plasma and/or the neutron flux due to the fusion reactions. These harsh conditions are of major concern, as hydrogen is known to alter the properties of materials, and loss of radioactive inventory is problematic in terms of both resource scarcity and conforming to regulatory constraints [7]. High energy ions and neutrons create displacement cascades leading to defects in the microstructure which, in the low fluence limit, are clusters of both vacancy and interstitial atom types. These defects can be trapping sites for hydrogen isotopes, increasing the retention and permeation properties of tritium. Further traps arise as a consequence of complex microstructure of Eurofer with grain boundaries, interfaces and possible precipitates of steel components, such as for example C, N, and O.

In this paper, we describe the experiments performed within the TRiCEM project investigating hydrogen isotopes interaction with fusion relevant first wall materials for DEMO. The ion exposure facility has been built and commissioned with helium and deuterium plasmas. Samples of Eurofer and Fe–Cr model alloy have been exposed in the facility after several levels of damage have been created in them by self-ion implantation in the University of Helsinki's ion beam laboratory. For this project we are able to combine TDS, SIMS, TEM, and other characterization methods to study the deuterium retention and the defect creation as a function of the level of damage and their evolution with time and temperature.

The paper is organized as follows. In section 2, hydrogen isotope exposure facility is described in detail, and benchmarking results are reported. In section 3, we present the results of TDS, SIMS, and TEM analysis of irradiated and exposed Eurofer and Fe–Cr samples. We discuss results on overall deuterium inventory, its time dependence, and the TDS peaks, and conclude in section 4.

2. Hydrogen isotope exposure facility

2.1. Facility

A major component of the TRiCEM project has been the design and build of a tritium capable ion exposure materials facility. Most of the development work was completed by H3AT (Hydrogen-3 Advanced Technology) staff at the UKAEA. The exposure to ions is performed within a custom ultra-high vacuum (UHV) implantation system. This will include a self-contained tritium handling system. For the initial deuterium work a scaled down gas handling system is used and the deuterium gas is re-circulated through the system in the same way as the tritium gas is required to be re-circulated. This ensures the deuterium and tritium results will be consistent. During the inactive stage of the experiment it is also possible to use the deuterium in a 'once through' fashion where the exhaust is vented rather than re-circulated. This once through method is more comparable to techniques that are typically employed by other existing experiments.

The primary purpose of this ion exposure facility is to expose material samples to hydrogen ions, including tritium. The level of exposure must be sufficient for the analysis techniques employed, primarily TDS and SIMS, to measure the retention levels. The fluence should be high enough to enable exposures to be completed within a single working day. The ion energy should be below the threshold required to induce significant microstructural damage.

The ion exposure facility is composed of a sample loading chamber and load lock system to allow sample handling within a vacuum and to ensure potential tritium contamination is minimized as far as is practical. The sample stage has both a cooling and heating system for accurate temperature control in the range 4 °C–450 °C. The low energy ions (50 eV–2 keV) are generated in a boron nitride plasma chamber surrounded by an 86 mT multi-polar magnetic array which provides electron cyclotron resonance to allow a higher density plasma to be created. A 2.45 GHz radially symmetric microwave field is used to produce the plasma. Ions are extracted from the plasma and focused onto the sample by two high voltage plates, each with a series of 1.95 mm diameter holes. The arrangement of holes on the inner grid provides an aperture of 13 mm diameter. The system is housed within a glovebox with an interlocking activity monitor. High quality welding and components are used throughout to ensure tritium compliance. The dry scroll pump used for this project is a special prototype being developed for tritium use with Edwards Vacuum Limited.

The system used for the deuterium work to date is shown below in figure 1. The system includes data acquisition to record ion exposure and other conditions during exposure as well as some ancillary sections for sample storage in vacuum and inventory storage or purification. The inventory can be stored in a solid state on the SAES CapaciTorr® HV200 pump which uses a ZAO getter alloy. A zeolite chamber is filled with 1/8″ zeolite pellets. The main purpose is to dry the gas inventory, but zeolite is also capable of removing other potential impurities. The gas inventory is expected to include very low traces of water vapor as it is possible to generate water in a hydrogen plasma system when oxides are present. A Hamamatsu C10083CAH spectrometer is used to monitor the plasma chamber and deviations from the expected deuterium spectrum can indicate trace impurities building up in the deuterium inventory.

The commissioning of the system with deuterium has been used to measure the ion flux under typical exposure conditions. The variables affecting ion flux are the exposure chamber pressure (within the range 5×10^{-3} mbar to 2×10^{-2} mbar,

Figure 1. Plasma exposure system after inactive gas commissioning. The system is partially built into the secondary containment system which will be required for tritium commissioning.

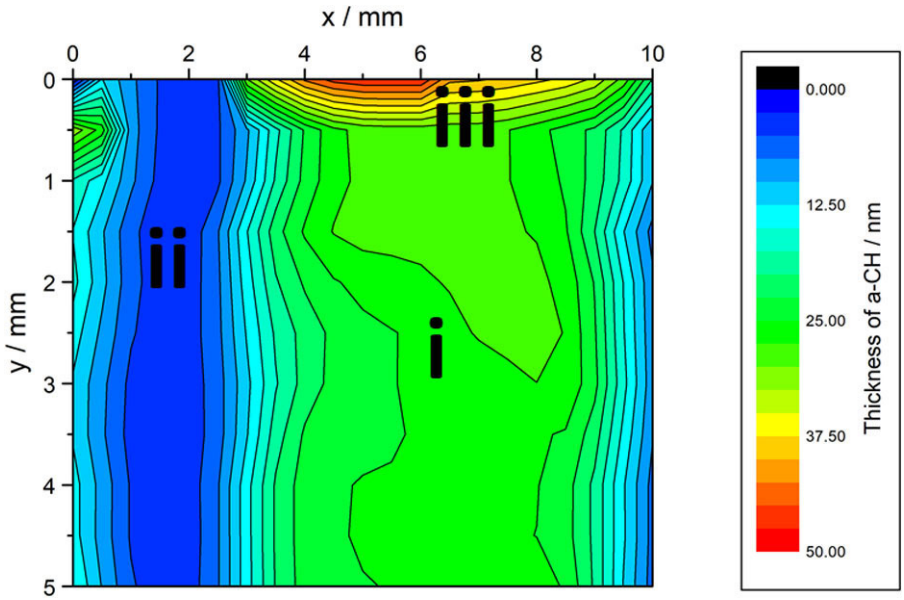

Figure 2. An ellipsometry survey of an a-C:H foil exposed to 100 eV deuterium ions for 20 min. Region (i) shows approximately uniform erosion by the beam in the central area where the sample is located. Region (ii) shows where the left-hand retaining clip held the foil in place, and similarly the imprint of the right-hand clip can be seen to the right of the figure. Region (iii) shows where the top of the foil was shielded from the ion flux by a molybdenum foil shield and so the amount of erosion reduces sharply.

typically 9×10^{-3} mbar) the current supplied to the magnetron (within the range 11 mA to 70 mA, typically 40 mA), the voltage of the anode (within the range 0 V to 2 kV, typically 400 V) and the voltage of the extractor (within the range 0 V–1 kV, typically −200 V).

The flux is not expected to be spatially uniform and the angular distribution of the ion source was measured using two complementary methods. During sample exposures the ion current impinging on two areas is measured using Keithley model 2100-6 multimeters and a comparison is made to indicate the approximate beam divergence. Ellipsometry measurements are also used to determine the erosion of an amorphous, hydrogenated carbon (a-C:H) film placed over the sample area. This erosion technique has been demonstrated to measure the angular distribution of hydrogen beams in [8]. Figure 2 shows an ellipsometry survey from a 20 min exposure to 100 eV deuterium ions with the sample stage held at 650 K. The central area where the beam is incident has approximately uniform erosion.

The approximately uniform erosion in the central region shown by the ellipsometry survey is expected when considering the 13 mm diameter aperture used for the anode of the ion source which is centered over the sample stage, where the sample holder plate is 18 mm × 15.5 mm with a

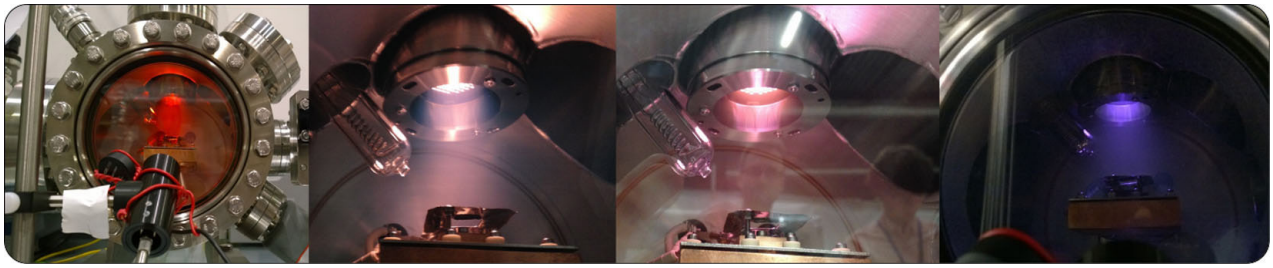

Figure 3. Photographs of commissioning plasmas. From left to right these are neon, helium, air and argon. The divergence of the ion beam can be observed.

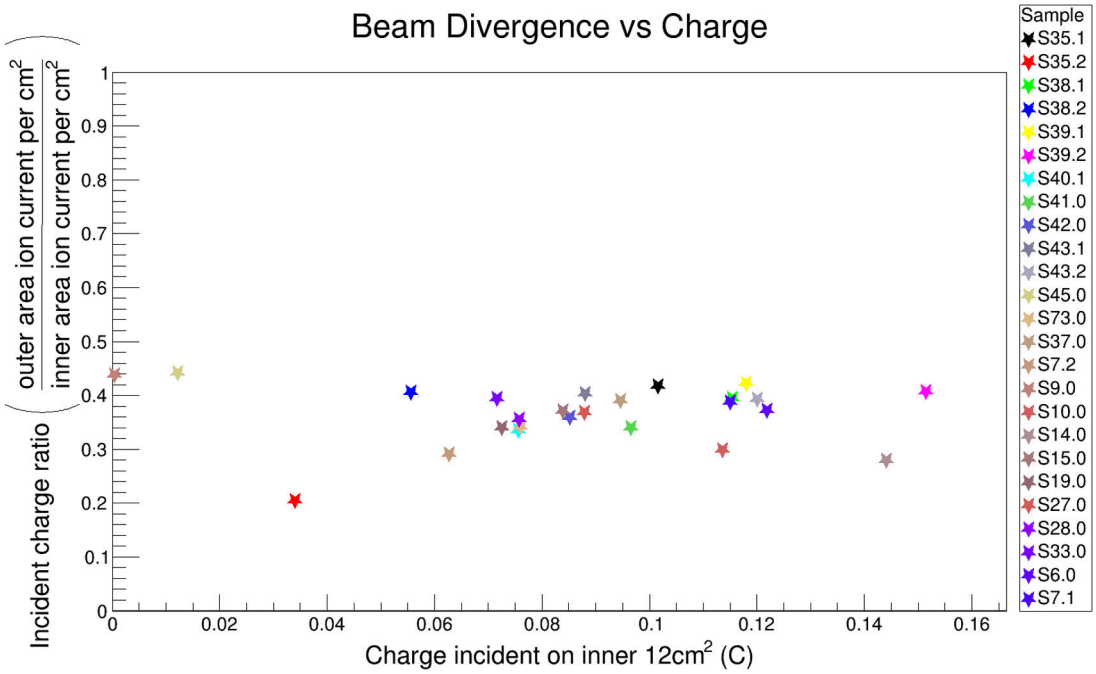

Figure 4. The ratio of ions incident on the inner and outer plates, providing an indication of beam divergence. The ratio of the areas of these plates is 0.7.

9 mm × 11.5 mm sample seat in the center. Away from the region directly underneath the aperture the beam is less uniform. This can be observed by eye, as shown in figure 3, and is also shown by incident current measurements on the inner and outer areas where the ions land. The area of the outer part is 17 cm^2. The inner area, which includes the sample, is 12 cm^2 and so the area ratio is approximately 0.7. Figure 4 shows a ratio of the average current incident on each area against the total charge incident on the inner area during the exposure of 25 samples, where the measured charge in the inner area is related the total number of ions incident on the sample. The ion beam lands as a cone and these plates are approximately square, so the ratio does not relate directly to beam divergence.

Although the ratio shown in figure 4 is calculated using much larger areas than the central area of interest (typically only the inner ~1 cm^2), this value is useful to confirm a consistent divergence of the beam between different exposures, since the divergence is variable depending on the ion source parameters and the chamber conditions.

The measured ion current during the exposure can be used to estimate the total fluence. The estimated ion fluence can be compared to the total retention measured by TDS and cross-checked against literature values for the expected deuterium uptake in the undamaged materials used for commissioning the system. During commissioning, several undamaged tungsten samples were exposed and sent for TDS analysis with a range of time intervals between the exposure and TDS analysis, as the delay period was found to be a significant factor in the measured total retention. Tungsten samples were selected here to allow comparisons with existing literature.

2.2. Benchmarking

The undamaged tungsten sample S38 was exposed over two consecutive working days for a total of 8 h. Overnight operation is not currently permitted in the facility, so the exposure was halted overnight. Standard tungsten exposure conditions were used (40 mA magnetron power, 400 V on the anode and −200 V on the extractor with a plasma chamber pressure of 1 Pa and a sample stage temperature of 50 °C). A gap of 2 d was then left before the TDS analysis began. The TDS used a ramp rate of 10 K min^{-1} from ambient temperature to 1000 °C, where the sample was held at the maximum temperature for

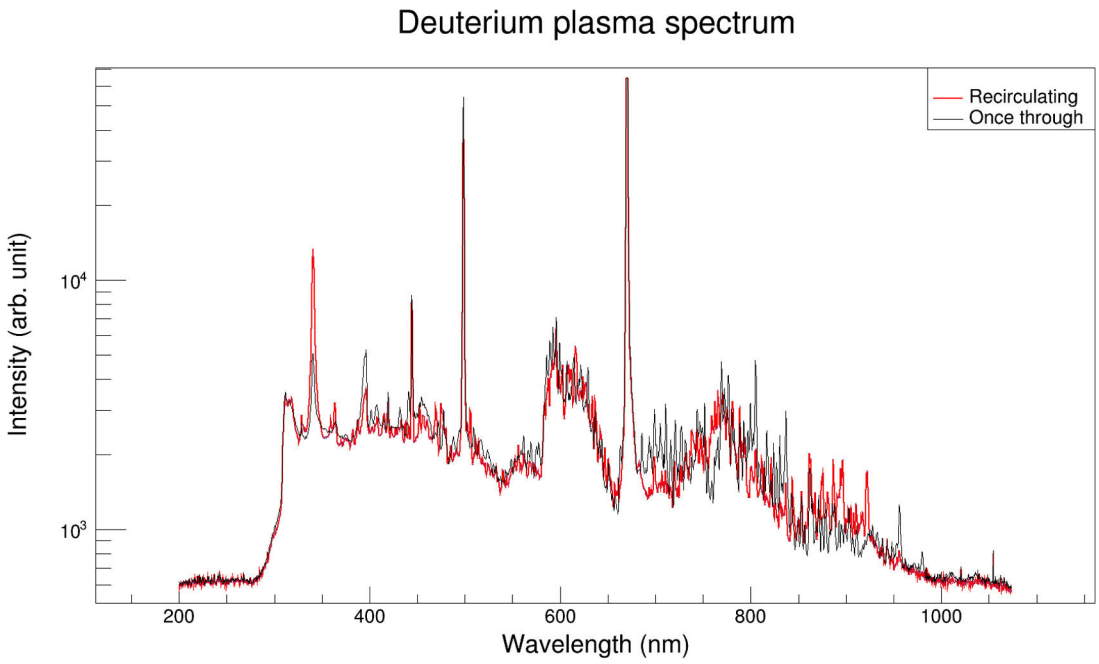

Figure 5. A comparison of spectra taken using recirculating and 'once through' deuterium. The D_β and D_α lines can be seen at 486 nm and 656 nm respectively, along with the Fulcher band between 560 nm and 640 nm. The recirculating spectrum indicates no significant build-up of impurities caused by recirculation of the deuterium through the plasma chamber, suggesting deuterium results can be compared with those from other systems which typically have a 'once through' setup and exhaust the deuterium from the exposure chamber. Tritium gas cannot be exhausted, so this result also indicates that the tritium results obtained with this system in the future can also be compared with other literature results.

1 h. For calibration, a reference sample method was used as described in [9]. The species considered were D_2 (atomic mass 4) and HD (atomic mass 3). The contribution of D from other mass numbers such as (HDO, atomic mass 19) was found to be negligible. Calibrated leak method [10] was used to confirm the reference sample method, and the results obtained were almost identical. The total deuterium retention was measured at 5.81×10^{19} D m^{-2}. The total charge measured on the 12 cm^2 sample stage was 2.13 C. Measurements of the ion species fractions were not made for this system, however measurements of ions produced in a similar way show approximately 0.97 D_3^+, 0.02 D_2^+ and 0.01 D^+ [11] suggesting an average of 2.96 deuterium atoms per incident ion and energy per ion, determined by anode potential (400 V) and number of atoms to be about 133 eV per atom. The lower limit of the fluence can be calculated by assuming the beam profile is uniform over this central part of the sample stage which falls directly below the aperture. For this example sample, the fluence is at least 8.74×10^{21} D m^{-2}. Accounting for the exposure time the ion flux in this region is 3.04×10^{17} D m^{-2} s^{-1}.

For high-purity tungsten, retention of deuterium was measured for several valued of incident fluence in [12]. The energy of D ions corresponded to 200 eV per deuteron, close to the one used in the current study. With flux being about two order of magnitude higher ($2.5–5 \times 10^{19}$ D m^{-2} s^{-1}), overall retention at fluence close to 10^{22} D m^{-2} was between 2×10^{19} and 10^{20} D m^{-2} ([12], figure 3), i.e. our results fall well within this range. Further measurements of the dependence of retention on the flux in undamaged tungsten alloy samples [13, 14] show that the fraction of retained deuterium is expected to be between 0.5×10^{-4} and 2×10^{-4} for a flux of ~10^{21} D m^{-2} s^{-1} (see [12], table 2). The example sample used here has a retention fraction of 0.0066, almost two orders of magnitude higher. This apparent discrepancy can be explained when considering the strong dependence of the retention on the ion fluence. With retention R proportional to $F^{0.5}$, where F is fluence [12–14], retention to fluence fraction should behave as $R/F \sim F^{-0.5}$, thus decreasing with the fluence. With fluence in [13, 14] being about 10^{25} D m^{-2}, nearly three orders of magnitude higher than in our experiments, retention to fluence ratio should fall by more than 10 times. Next, the flux of 3×10^{17} D m^{-2} s^{-1} calculated for this system is a lower bound, as the beam is likely to be denser towards the central region where the sample is located. Finally, the ion energy used for S38 is 133 eV per deuteron, whereas 40–60 eV was used in [13, 14] and our sample S38 was high purity tungsten, like in [12], rather than the W–Ta alloy used in [13, 14].

During sample exposure several measurements are recorded to ensure consistency. In addition to the ion current measurements these are: optical spectroscopy of the plasma emission lines, optical power output between 400 nm and 1100 nm, the sample stage temperature and various pressure readings. Optical spectroscopy is used to monitor the impurity build up in the deuterium inventory. The silicon diode optical power meter monitors the stability of the ion source during the exposure, as do the pressure readings, and the sample stage temperature is required for the automated temperature control system.

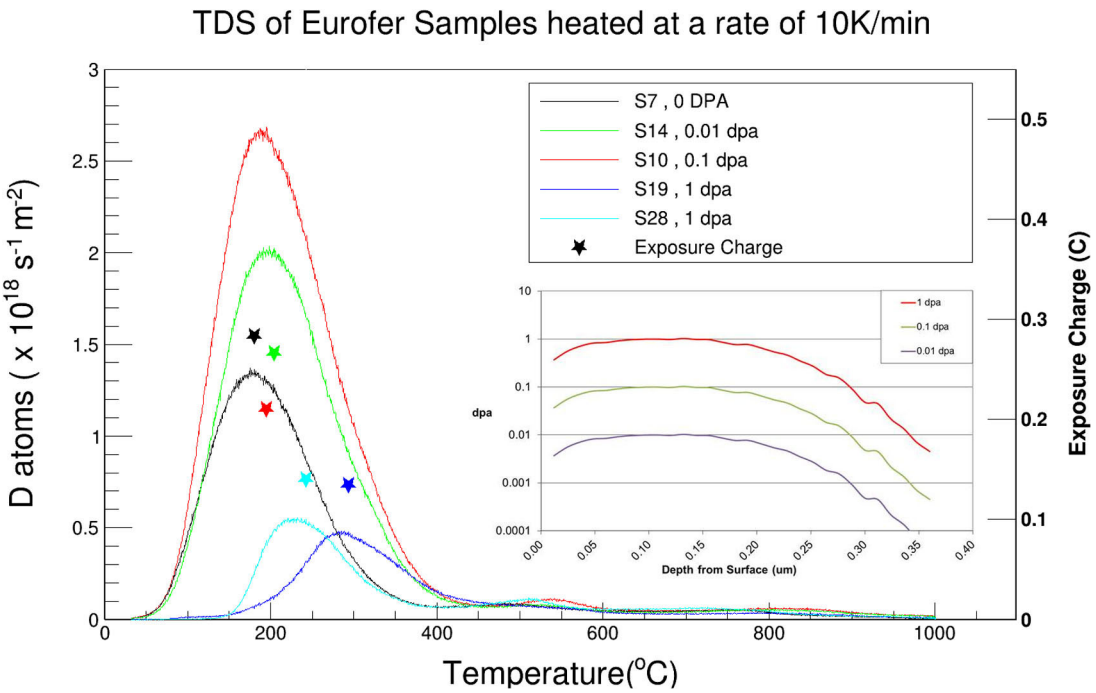

Figure 6. TDS spectra of deuterium and exposure charge in Eurofer samples with damage levels between 0 and 1 dpa. Time period between exposure to deuterium plasma and the TDS is 1 d for all samples. The lower limit of the charge incident on the sample is indicated. It can be seen that the retention is more strongly affected by the damage level than the ion fluence. Inset shows damage as function of depth calculated using SRIM program.

In tritium experiments, the tritium inventory will be recirculated through the plasma chamber. In order to ensure current deuterium results are consistent with future tritium results the deuterium inventory is also recirculated. A spectrometer is used to measure the deuterium purity over time to ensure the results are not skewed by significant formation of hydrocarbons and water. Figure 5 shows typical spectra observed with a Hamamatsu C10083CAH spectrometer (spectral range from 320 nm to 1000 nm) after transmission through a Kodial viewport (transmission is above 85% for this range). The spectrum plotted with a red line was taken during the exposure of a tungsten sample in recirculating mode, the black line shows a 'once-through' mode spectrum where the deuterium is exhausted. The deuterium used in recirculating mode had previously recirculated through the plasma chamber for 45 h during exposures of Eurofer and W samples. Recirculating deuterium had not been exposed to zeolite or ZAO getter during this period. The key lines of expected impurities (which do not overlap with deuterium lines) are not present. These are CH (425 nm), C_2 (516 nm), and O (777 nm and 845 nm) emission lines.

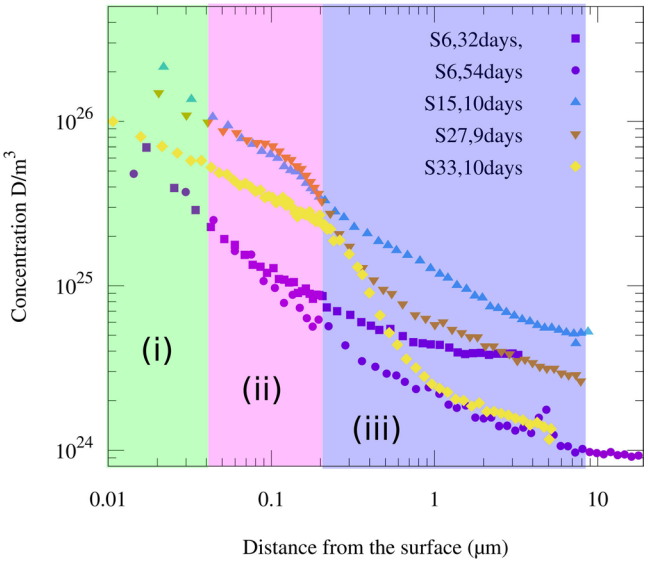

Figure 7. SIMS depth profiling of deuterium content of damaged Eurofer samples. Irradiation doses: S6—0 dpa, S15—0.01 dpa, S27—0.1 dpa, and S33—1 dpa. Labels (i), (ii), and (iii) correspond to the surface, damaged, and bulk regions, respectively. Time delay between exposure to deuterium plasma and the SIMS is given in days.

3. Results

3.1. Eurofer

Production of Eurofer and Fe–Cr samples for the TRiCEM project involves sourcing high purity certified materials which are cut using electrical discharge machining. The samples were ground using SiC paper (P250–P4000) before being polished with a diamond and colloidal silica. The polished samples have been cleaned in an ultrasonic bath with acetone and isopropanol. No heat treatment was performed, because annealing above 600 °C causes irreversible changes of the microstructure and permanent loss of the mechanical properties of steels. Prepared samples were shipped to the accelerator laboratory at the University of Helsinki where high energy ions are used to damage the microstructure. Irradiation was performed using raster-scanned beam at room temperature. The ion species used for this work are 0.5 MeV Fe^+ and

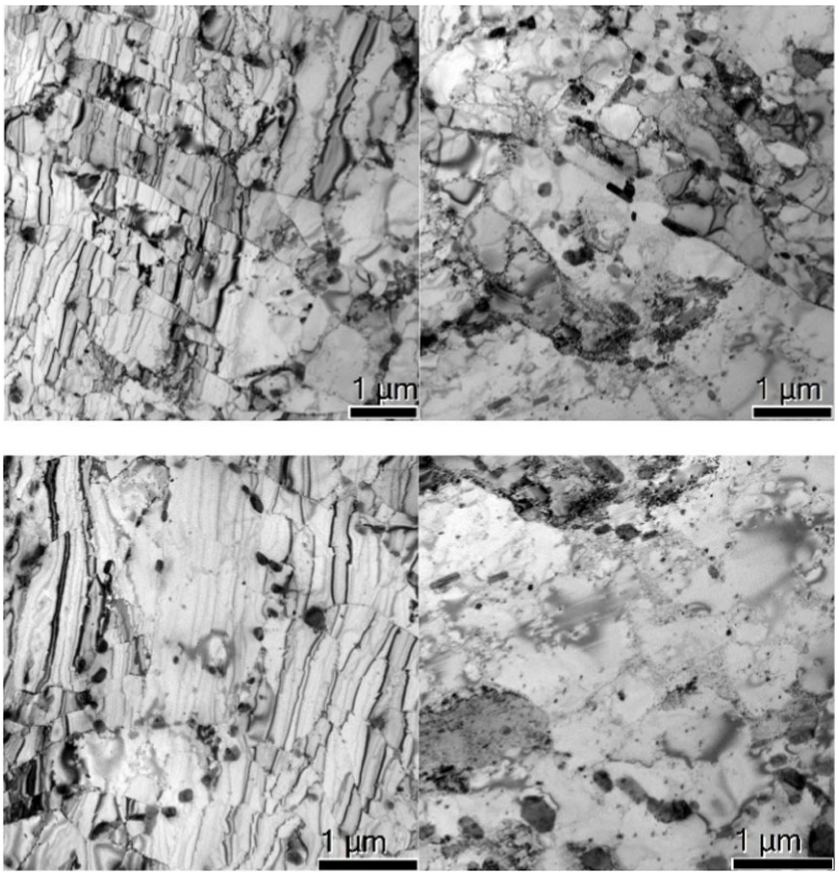

Figure 8. Bright field TEM images of the Eurofer before irradiation and exposure.

the fluences used were $3.2 \times 10^{16/17/18}$ ions cm^{-2} for damage levels of approximately 0.01/0.1/1 dpa respectively. The irradiation levels were calculated using SRIM software [15–17] with 'Detailed Calculation with full Damage Cascades' option. After exposure to deuterium plasma up to an estimated fluence of 10^{23} D m^{-2} (plasma temperature 50 °C, ion energy 400 eV), TDS analysis was performed by the UKAEA. The samples were heated to 1000 °C with a constant rate of 10 K min^{-1}, and the amount of hydrogen and deuterium was counted. Figure 6 shows deuterium spectra as a function of temperature and the total exposure charge (overall charge of D ions), with calculated damage as function of depth shown in the inset. SIMS analysis of the samples was performed in VTT, Finland, and TEM at CEA Saclay, France.

TDS spectra (figure 6) demonstrate the existence of three peaks of different heights. The first peak is situated between 150 °C and 200 °C for samples irradiated below 1 dpa. The release of deuterium in this peak begins at temperatures just above 50 °C, i.e. just above the exposure temperature. For the 1 dpa samples, the first peak is much lower and shifted to higher temperatures of about 220 °C–300 °C. The second peak at about 500 °C–550 °C is much smaller than the first. The very weak third peak was found at approximately 800 °C.

For the purposes of analysis of SIMS results on the penetration of deuterium in the samples, the surface layer was divided into three regions: the surface (i) of 0.04 μm thickness, the damaged (ii) between 0.04 and 0.2 μm depth, and the bulk (iii) between 0.2 and 8 μm. The range of the damaged region was chosen so that the damage according to the SRIM calculations (figure 6, inset) was at least 0.75 of the maximum damage. Distribution of deuterium in these regions is shown in figure 7. The deuterium concentration in the damaged region increases up to 0.1 dpa. For the damage level of 1 dpa, however, the concentration and penetration depth of deuterium decreases compared to the 0.01 and 0.1 dpa samples, thus confirming similar decrease found in TDS spectra. Deuterium inventory in unirradiated sample S6 is lower than in all irradiated samples, because of three to five times longer delay between exposure and SIMS.

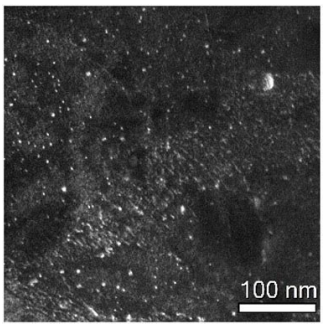

Figure 9. Weak beam dark field image of the Eurofer at room temperature after irradiation and exposure to deuterium ($g = 110$).

The samples have been characterized by TEM prior to and after irradiation and deuterium exposure. They were mechanically polished by silicon carbide/diamond abrasives to 100 μm thickness, using a Struers grinding/polishing machine. Then,

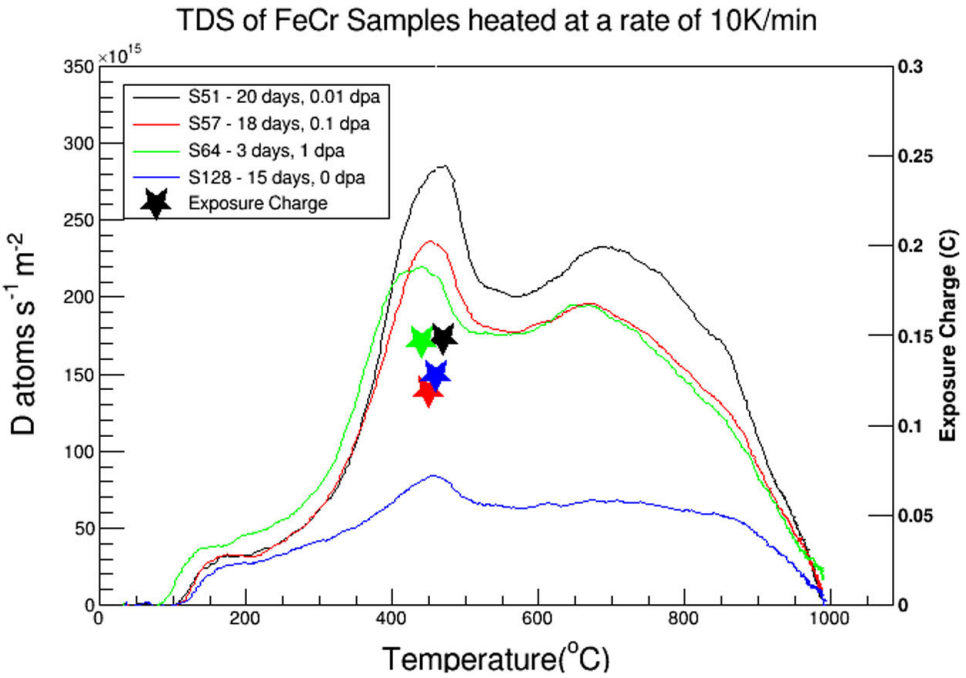

Figure 10. TDS spectra of deuterium in Fe–Cr samples with damage levels between 0 and 1 dpa. Irradiation doses: S128—0 dpa, S51—0.01 dpa, S57—0.1 dpa, and S64—1 dpa.

discs of 3 mm diameter were punched out and electropolished for a few seconds to obtain mirror finished dimpled discs in a Tenupol-5 thinning device. These discs were then irradiated and exposed to deuterium. After irradiation and deuterium exposure, the discs were thinned again protecting the irradiated side with a protective varnish. *In situ* TEM annealing has been performed with the same constant rate of 10 K min^{-1} as TDS from room temperature to 1000 °C using a Gatan 625 specimen holder.

Before irradiation, the material presented typical ferritic/martensitic microstructure composed of equiaxed grain/subgrain structure (figure 8). It also included groups of laths within the prior austenitic grains. Some incipient formation of equiaxed grains (alignment of dislocations) are visible. Large intergranular carbides are also present, as well small intragranular precipitates. Some of the large precipitates are facetted.

After irradiation to 1 dpa and deuterium exposure, some dislocation loops are present at room temperature (figure 9). They grow during *in situ* annealing between 813 and 1013 K (540 °C–740 °C), i.e. at temperatures close to and just above the temperature of the second peak in TDS. Cavities were not present or were below the visibility threshold (around 1 nm).

3.2. Iron–chromium alloy

TDS analysis of model Fe–Cr alloys with chromium content of 8 weight % was performed in Forschungszentrum Jülich, Germany, with time delay between exposure and the TDS ranging between 3 and 20 d. This differs from the case of Eurofer, where all samples were analyzed 1 d after the exposure; however, several important conclusions can be made. TDS spectra (figure 10) show a rapid rise of deuterium content in irradiated samples (S51, S57, S64) compared to an unirradiated one (S128), with the total amount of absorbed deuterium almost independent of the dose. Total deuterium inventory in unirradiated sample was found to be 1.93×10^{20} D m^{-2}, for irradiated samples it was 5.59×10^{20} D m^{-2} (0.01 dpa), 4.83×10^{20} D m^{-2} (0.1 dpa), and 5.15×10^{20} D m^{-2} (1 dpa). Note though that for the 1 dpa sample S64, TDS was performed only 3 d after the exposure, and it is in the low-temperature range that deuterium inventory is higher in that sample than in others. Longer delay would probably result in further inventory decrease for that sample. Similar to the case of Eurofer, several main peaks can be identified: at around 150 °C, 450 °C–500 °C, close to 700 °C, and possibly around 800 °C. The first peak is much lower compared to the high temperature peaks, unlike the case of Eurofer. Also, the first peak changes very little with irradiation dose, while the second and third peaks rise sharply for irradiated samples compared to the unirradiated one. Rapid saturation of total deuterium inventory and absence of its significant fall at dose of 1 dpa are further differences between Fe–Cr alloy and Eurofer.

SIMS analysis of Fe–Cr samples was performed after between 55–59 d after exposure. The results shown in figure 11 show a substantial decrease in deuterium content in damaged regions for sample irradiated to 0.01 dpa compared to doses of 0.1 and 1 dpa. This strongly indicates that higher irradiation dose results in slower inventory decrease with time, similar to the case of Eurofer (see below, figure 12). Again, direct comparison with SIMS on Eurofer samples is difficult because of different time delays between exposure and analysis; still it is worth mentioning contrast with almost equal content of deuterium in damaged zone of Eurofer for doses of 0.01 and 0.1 dpa (figure 7).

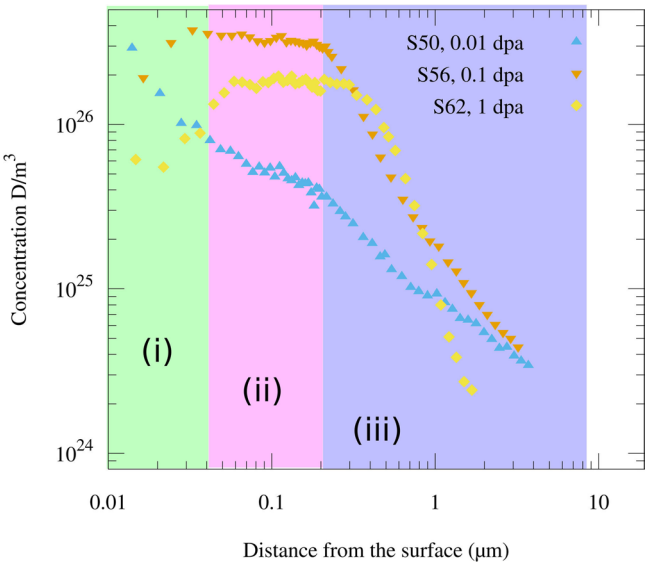

Figure 11. SIMS depth profiling of deuterium content of damaged Fe–Cr samples. Labels (i), (ii), and (iii) correspond to the surface, damaged, and bulk regions, respectively. For S50, S56 and S62 the delays were 59, 55 and 57 d, respectively.

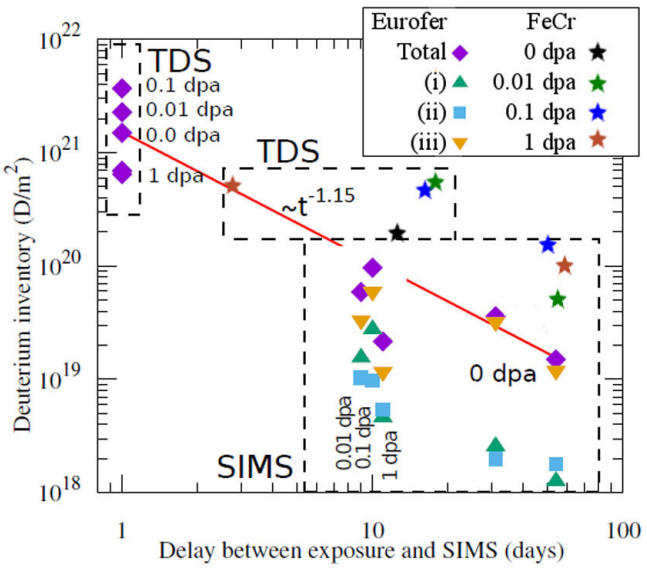

Figure 12. The total retention in Eurofer and Fe–Cr samples as a function of delay between exposure and analysis. For Eurofer samples, the inventory in surface (i), damage (ii), and bulk (iii) regions is also shown.

4. Discussion and conclusions

Overall deuterium retention for all samples studied is shown as a function of time between exposure and analysis in figure 12. The straight line corresponds to the dependence of total inventory of deuterium in unirradiated samples of Eurofer. The time dependence for that line is close to inversely proportional (exactly, it behaves as $t^{-1.15}$). This exponent is consistent with similar experiments on tungsten [18], where exponents between −0.7 and −1.1 were found for outgassing at room temperature. Further, comparison of the decrease of inventory for different irradiation doses shows that for both Eurofer and Fe–Cr alloy, higher dose results in slower decrease.

The first peak at 150 °C–200 °C corresponds to release of deuterium from the weakest traps or the interstitial positions. Comparison of TDS in Eurofer and Fe–Cr shows that this peak is considerably lower in Fe–Cr. This could be due to release of deuterium during the delay between exposure and the TDS, as well as it moving to stronger traps. In order to check this, further experiments on Fe–Cr with minimal delay are necessary. The position of the first peak (150 °C–200 °C) should be compared with recent similar experiments. Exposure to low energy 40 eV deuterium ions resulted in peak at 290 °C [19], similar peak temperature was found for 20 eV ions [20, 21]. Exposure to high energy 5 keV D_3^+ ions, on the other hand, results in a peak at about 130 °C–170 °C [22]. Our results were obtained after exposure to 400 eV ions, i.e. the energies are intermediate between those in [19–22]. They confirm the trend of decreasing temperature of the first peak with increasing energy of deuterium ions.

Two Eurofer samples irradiated to 1 dpa show similar differences from lower dose samples: substantial decrease in deuterium inventory and a shift of the first peak to higher temperatures (220 °C for S28, almost 300 °C for S19). The reasons for the decrease of inventory are not clear at this point, however, the similarity in this behavior strongly suggests this is a genuine effect. One of the possible explanations could be acceleration of release of deuterium from surface and damage layers because of damage accumulation; however, this needs further investigation. The decrease is also confirmed by SIMS results that also demonstrate decrease of D content in 1 dpa samples, compared to 0.01 and 0.1 dpa. It was found in [21] that irradiation with 20 MeV W ions results in saturation of deuterium concentration at a peak damage at about 0.5 dpa, with the same concentration up to ~3 dpa. Still, the direct comparison between our results and those obtained in [21] is difficult, because (i) there is no data on overall D retention as a function of irradiation dose in [21], (ii) our SIMS profiles (figure 7) do not show a maximum in D concentration with depth, and (iii) energies of irradiation ions in [21] are almost two orders of magnitude higher than in the present study (20 MeV versus 0.5 MeV). To clarify possible decrease of D inventory with dose, further experiments with samples irradiated to intermediate as well as higher doses are planned.

The second peak at around 450 °C–500 °C (720–770 K) in Eurofer and Fe–Cr is most pronounced in Fe–Cr. This peak can be associated with release of deuterium from vacancies or vacancy cavities. This possibility should be checked further by modelling H/D release from traps with binding energy about 0.57–0.6 eV that is characteristic for vacancies [23, 24]. It is worth noting that *in situ* TDS measurements performed 45 min after exposure did not reveal more than one peak up to 800 K [22]. Experiments performed with longer delay between exposure and TDS revealed second peak at about 790 K [20] or broad overlapping peaks at 730 and 900 K [19]. The third peak is very low in Eurofer, while in Fe–Cr a broad structure possibly consisting of more than one peak was found between 700 °C and 900 °C. This broadening may be due to the fact that because of longer time delays between exposure and analysis, deuterium penetrated deeper in Fe–Cr, as observed in

the SIMS profiles. Note that it is not obvious that the mobility of deuterium in Fe–Cr and Eurofer is the same.

Summarizing, the first results obtained from the tritium capable ion implantation materials facility in UKAEA (Culham, United Kingdom), are presented in this paper. TDS, SIMS, and TEM study of Eurofer was performed and increase in deuterium retention with increased irradiation dose up to 0.1 dpa was observed with subsequent fall for 1 dpa samples. The TDS study of Fe–Cr alloy was performed for the first time, to the best of our knowledge. Here, the increase of deuterium content quickly reaches a plateau for Fe–Cr alloy, remaining at approximately the same level for all irradiation doses studied. Peaks in the TDS spectra are associated with the release of most of the deuterium from interstitials, vacancies, cavities, and possibly the grain boundaries. Time delays between exposure of samples to deuterium plasma and subsequent TDS/SIMS analysis evidently result in considerable loss of total deuterium retention, especially in the case of Fe–Cr alloy. Several notable differences are noticed between Eurofer and Fe–Cr. While some of them may be due to different time delays between exposure and analysis, other, such as deuterium retention as function of dose, might be genuine and require further studies. The results obtained in this study with deuterium will be checked by adding intermediate irradiation doses and will be compared to tritium behavior when full tritium operation of the facility becomes possible.

Acknowledgments

We thank M. Rieth for his help providing the material for the Eurofer samples and T. Schwartz-Selinger for many useful discussions and advice, and for providing a-C:H foils for beam characterization. Some of the research used equipment at the UKAEA's Materials Research Facility (MRF) which is part of the UK's Henry Royce Institute and National Nuclear User Facility initiatives. We thank the MRF staff for their support. This work was supported by EUROfusion Enabling Research project TRiCEM, Tritium Retention in Controlled and Evolving Microstructure and part-funded by the EPSRC Program (Grant No. EP/P012450/1). This work has been carried out within the framework of the EUROfusion Consortium and has received funding from the Euratom research and training program 2014–2018 and 2019–2020 under Grant agreement No. 633053. The views and opinions expressed herein do not necessarily reflect those of the European Commission. To obtain further information on the data and models underlying this paper please contact PublicationsManager@ccfe.ac.uk.

ORCID iDs

A. Hollingsworth https://orcid.org/0000-0002-2251-506X
M.Yu. Lavrentiev https://orcid.org/0000-0001-9899-1700
R. Watkins https://orcid.org/0000-0001-6467-2891
A.C. Davies https://orcid.org/0000-0001-6697-3831
S. Davies https://orcid.org/0000-0002-7760-0675
D.R. Mason https://orcid.org/0000-0002-1536-6254
A. Baron-Wiechec https://orcid.org/0000-0001-9458-6679
I. Jepu https://orcid.org/0000-0001-8567-3228
K. Heinola https://orcid.org/0000-0002-0601-8274
K. Mizohata https://orcid.org/0000-0003-1703-2247
E. Meslin https://orcid.org/0000-0003-0357-4256
M.-F. Barthe https://orcid.org/0000-0002-0170-9498
A. Widdowson https://orcid.org/0000-0002-6805-8853
I.S. Grech https://orcid.org/0000-0002-3133-4711
A. McShee https://orcid.org/0000-0002-2850-1857

References

[1] Riccardo V. *et al* 2013 *Fusion Eng. Des.* **88** 585–9
[2] Merola M. *et al* 2014 *Fusion Eng. Des.* **89** 890–5
[3] Ueda Y. *et al* 2014 *Fusion Eng. Des.* **89** 901–6
[4] Rieth M. *et al* 2013 *J. Nucl. Mater.* **432** 482–500
[5] Zinkle S.J. *et al* 2017 *Nucl. Fusion* **57** 092005
[6] Brezinsek S. *et al* 2017 *Nucl. Fusion* **57** 116041
[7] Lipschultz B. *et al* 2010 *Report* PSFC/RR-10-4 MIT
[8] Schwarz-Selinger T., von Keudell A. and Jacob W. 2000 *J. Vac. Sci. Technol.* A **18** 995–1001
[9] Baron-Wiechec A. *et al* 2018 *Fusion Eng. Des.* **133** 135–41
[10] Avotina L. *et al* 2019 Thermal desorption of hydrogen isotopes from the JET Be plasma facing components *Phys. Scr.* accepted (https://doi.org/10.1088/1402-4896/ab3c38)
[11] Manhard A., Schwarz-Selinger T. and Jacob W. 2011 *Plasma Sources Sci. Technol.* **20** 015010
[12] Ogorodnikova O.V. 2009 *J. Nucl. Mater.* **390–1** 651–4
[13] Zayachuk Y. *et al* 2011 *Fusion Eng. Des.* **86** 1153–6
[14] Zayachuk Y. *et al* 2011 *Phys. Scr.* **T145** 014041
[15] Ziegler J.F., Ziegler M.D. and Biersack J.P. 2010 *Nucl. Instrum. Methods Phys. Res.* B **268** 1818–23
[16] Stoller R.E. *et al* 2013 *Nucl. Instrum. Methods Phys. Res.* B **310** 75–80
[17] Ziegler J.F. 2015 Interactions of ions with matter www.SRIM.org
[18] Möller S. *et al* 2017 *Nucl. Fusion* **57** 016020
[19] Martynova Y. *et al* 2017 *Nucl. Mater. Energy* **12** 648–54
[20] Ogorodnikova O.V. *et al* 2017 *Nucl. Fusion* **57** 036010
[21] Ogorodnikova O.V. *et al* 2017 *Nucl. Fusion* **57** 036011
[22] Ryabtsev S.A. *et al* 2017 *Phys. Scr.* **T170** 014016
[23] Counts W.A., Wolverton C. and Gibala R. 2010 *Acta Mater.* **58** 4730
[24] Mirzaev D.A. *et al* 2014 *Mol. Phys.* **112** 1745